Article:
Hao, J, Zhang, K, Zhang, Z orcid.org/0000-0003-0204-3867 et al. (2 more authors) (2023) An Online Model-Free Adaptive Tracking Controller for Cable-Driven Medical Continuum Manipulators. IEEE Transactions on Medical Robotics and Bionics, 5 (3). pp. 623-635. ISSN 2576-3202

https://doi.org/10.1109/tmrb.2023.3291024

An Online Model-Free Adaptive Tracking Controller for Cable-Driven Medical Continuum Manipulators

Jianxiong Hao, Kai Zhang, Zhiqiang Zhang, Shuxin Wang, Chaoyang Shi

***Abstract*—Continuum manipulators have demonstrated promising potential for flexible access and complicated operation and thus have been emerging and introduced in robot-assisted flexible endoscopy. However, due to their inherent structural compliance and strong nonlinearities, developing an accurate and robust control framework remains challenging. This paper proposes a model-free control method based on the Model-Free Adaptive Control (MFAC) algorithm to accomplish the trajectory tracking for two kinds of continuum manipulators by solely utilizing the robotic system's real-time input/output data. The presented controller discretizes and dynamically linearizes the motion process of the continuum actuator to obtain a dynamic linearization data (DLD) model. This DLD model can be derived from a pseudo-partial derivative (PPD) matrix updated based on the I/O measurement data for the iterative operation. The stability of the presented MFAC controller can be mathematically guaranteed in theory to provide generality, and the control framework demonstrates a low computational cost and real-time control capability. The superior performance of the presented controller is firstly validated in MATLAB simulations and then compared with the other two controllers. Through experimental validation on two kinds of continuum manipulators, the model-free control framework shows high tracking accuracy and good robustness against the system uncertainty and external disturbances, as well as high transferability.**

***Index Terms*—Continuum robots; model-free control; flexible endoscopy; minimally invasive surgery**

I. Introduction

Robotic-assisted flexible endoscopy that combines advanced robotic technology and endoscopic techniques has been increasingly introduced and accepted for both diagnostic and therapeutic functions and aims to realize the no-visible-scar surgical procedure [1], [2]. These relevant robotic systems demonstrate the potential and reliability in performing flexible internal inspection and complicated operations through natural orifices instead of noticeable skin incisions from keyhole surgery and open surgery [3]–[5]. Thus, these emerging techniques can reduce incisions and infection, intraoperative bleeding and pain, and recovery time for patients, lower fatigue and turnout for surgeons, and improve surgical outcomes and patient safety [6]–[8]. The cable-driven continuum manipulators have exhibited great potential and promising applicability for these robotic systems (e.g. EndoMaster System designed by Nanyang Technological University [9], K-Flex developed by KAIST [10], and Ion system developed by Intuitive [11]) due to their outstanding structural compliance, environmental adaptability, and flexible access capability in narrow cavities and tortuous anatomic pathways [12], [13]. However, these continuum manipulators commonly experience large and nonlinear deformation, complex friction, and significant hysteresis behaviors [14], [15]. The deformation is complicated for accurate prediction and control when the unknown external loadings or the curved environmental path is posed [16]. As a result, achieving the precise motion control of the continuum manipulators remains challenging. To improve control accuracy and stability, two typical frameworks that include model-based and model-free methods are generally proposed to control continuum robots [17], [18].

As for the model-based methods, both kinematics and dynamics models of continuum manipulators have been widely investigated. The constant curvature assumption is a frequently applied kinematic modeling method for continuum robots [19], [20]. Based on this theory, Li et al. developed a position feedback controller incorporated with a quadratic programming algorithm for a continuum robot and realized a smooth tracking path with a maximum error of less than 3 mm [21]. However, the computational costs of the Jacobian matrix are typically significant. Qi et al. proposed a fuzzy controller to perform the trajectory tracking of the distal tip position of an orthogonal planar spring-based continuum manipulator [22]. However, it is difficult to find a balance between the calculation costs and control accuracy to determine the number of fuzzy rules. Other approaches focus on the dynamic modeling of continuum manipulators based on the elastic beam theory and Cosserat-rod theory [23]–[25]. Till et al. employed a numerical framework for solving Cosserat rod-based dynamic models of different soft and continuum robots [26]. However, there typically exist large elastic deformation, strong nonlinearities for frictions and hysteresis, and unknown payloads for continuum robots. These make it challenging for this method to determine the accurate models for continuum robots. In conclusion, it is difficult to accurately identify the model parameters of model-based methods, and the complicated and changeable external environment typically leads to significant model inaccuracy and even failure. Therefore, the model-based method is unsuitable

Manuscript received July 4, 2022. This work is supported in part by National Natural Science Foundation of China under Grant 92148201, Grant 51721003, Grant 62211530111 and Grant 61973231, and Royal Society under IEC\NSFC\211360. Corresponding author: Chaoyang Shi (e-mail: chaoyang.shi@tju.edu.cn).

J. Hao, K. Zhang, S. Wang and C. Shi are with Key Laboratory of Mechanism Theory and Equipment Design of Ministry of Education, School of Mechanical Engineering, Tianjin University, Tianjin, 300072, China. Z. Zhang is with School of Electronic and Electrical Engineering, University of Leeds, Leeds, LS2 9JT, UK. This work is also supported by International Institute for Innovative Design and Intelligent Manufacturing of Tianjin University in Zhejiang, Shaoxing 312000, CN.

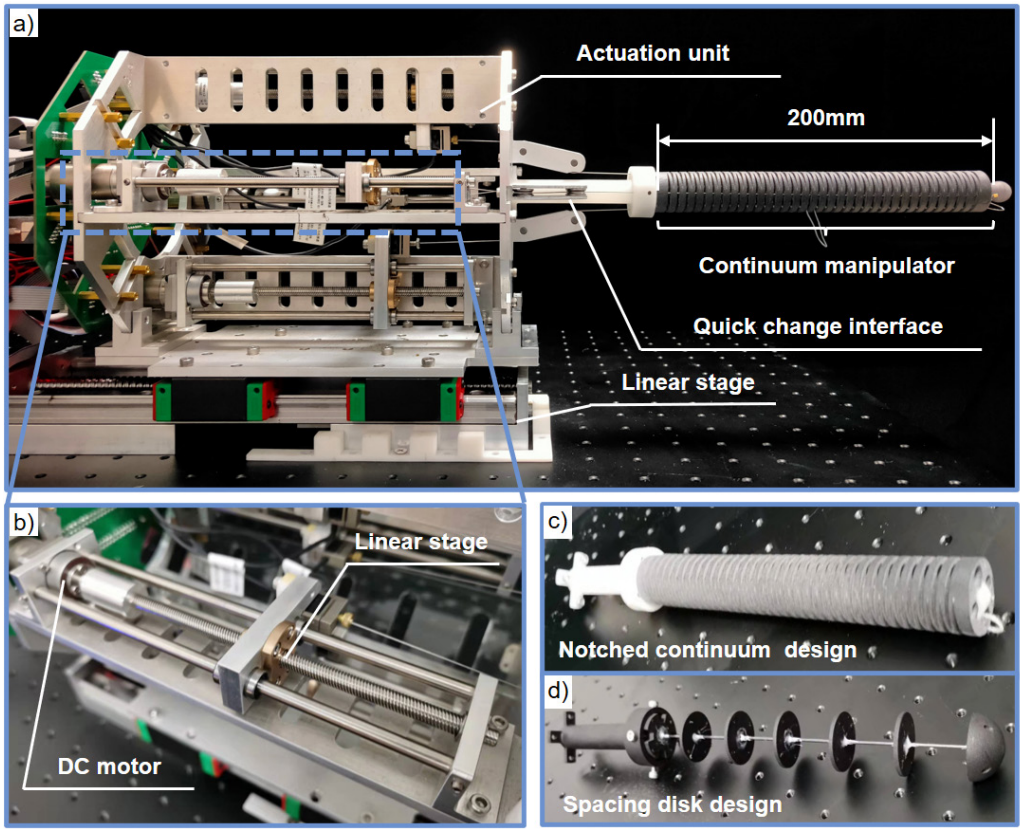

Fig. 1. a) The detailed design of the prototyped continuum robot; b) The DC motors connected with the linear modules; c) The notched continuum manipulator; d) The traditional spacing disk type manipulator.

for real-time control of continuum robots that dynamically interact with human tissues during surgery.

Without utilizing a specific model, model-free control algorithms based on offline learning or online state estimation are increasingly tempted and investigated to compensate for the uncertainties and nonlinearities of continuum manipulators. As for the method based on offline learning, Giorelli et al. utilized a feedforward neural network to solve the inverse statics of nonconstant curvature soft manipulators placed in water and obtained the mapping from the distal tip position to the cable tensions [27]. However, this method is only suitable in free space without loading and cannot be applied when existing friction and gravity. George et al. investigated a closed-loop kinematic controller based on machine learning and realized the end-effector position control of the cable-driven 6-DOF manipulator in the unstructured environment [28]. However, this method does not consider the dynamics of the continuum manipulator and increases the energy consumption in the control process. The offline learning methods need to re-collect data for training when the mechanical structure of continuum manipulators changes; thus, such methods suffer from poor transferability and lack of generality. Yip et al. presented a model-free closed-loop controller based on empirical estimation of the real-time Jacobian matrix of continuum manipulators for usage in constrained environments [29]. However, the usage of optimal algorithms results in high computational costs. Li et al. developed a model-free method based on an adaptive Kalman filter and performed the trajectory tracking of the continuum robot distal tip only based on the I/O measurement data [30]. However, this method is only suitable for quasi-static processes with relatively low speed and cannot be applied to the continuum manipulator's dynamic control.

To address the abovementioned issues, an online MFAC-based controller is proposed for the trajectory tracking control of continuum manipulators with stochastic external disturbances. The presented MFAC-based scheme is a data-driven and anti-disturbance control framework. The presented controller discretizes and dynamically linearizes the motion process of the continuum actuator to obtain a DLD model with a PPD matrix. By solely utilizing the robotic system's real-time I/O measurement data, the PPD matrix of the controller could be estimated online in every control loop by the modified projection algorithm. Compared with the offline learning methods, it does not require any data collection or training process. Besides, benefiting from the low computational cost, the proposed method could be simply and easily implemented for real-time applications. Moreover, the convergence and stability of the framework could be guaranteed, which is a highlighted feature compared with most model-free control approaches. Simulation and experimental results have shown that the proposed controller could achieve high tracking accuracy, strong robustness, and fast response toward the variable external disturbance. Meanwhile, the proposed controller has high transferability and can be utilized on the continuum manipulators of different designs.

II. Materials and Methods

A. Mechanical Design of the Continuum Robot

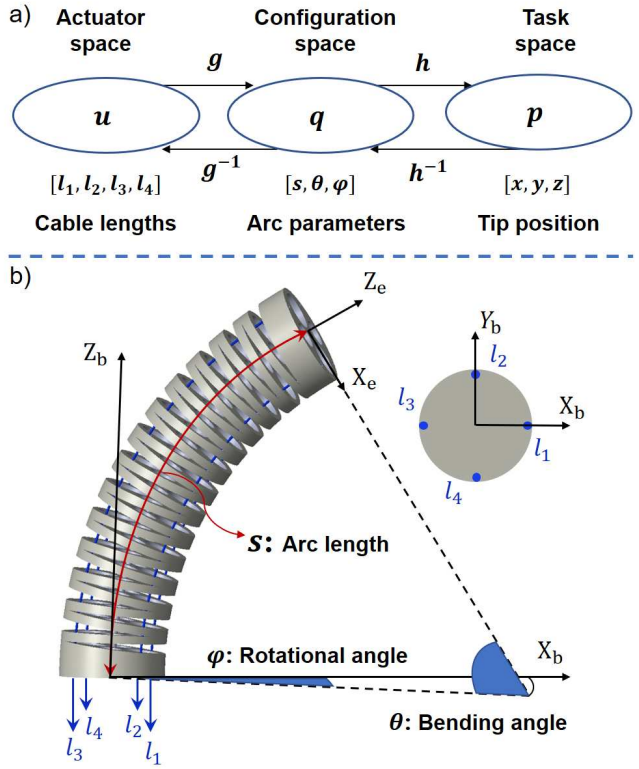

Fig. 2. a) Kinematic mapping relationship of a continuum manipulator based on the constant-curvature assumption; b) The configuration variables and different coordinate frames of the 2-DOF continuum manipulator bending in the 3D space.

The overview of the prototyped continuum robot has been illustrated in Fig. 1a), consisting of an actuation unit, a quick-change interface, and two kinds of continuum manipulators. The actuation unit is constructed with five DC motors (Maxon, DC16, Switzerland) mounted on five linear modules (Fig. 1b)). Four of them are utilized to drive cables to transmit displacement and force for continuum manipulator actuation. The remaining one provides the translational movement of the whole actuation module. Each linear stage consists of two side guide rails and a central lead screw arranged in parallel to maintain structural stability and reduce motion errors. The motors are equipped with encoders to record the cable displacement information. The quick-change interface is designed to support connecting different continuum manipulators with the actuation unit, improving the platform's versatility. Two kinds of 2-DOF medical continuum manipulators in terms of the notched continuum type (Fig. 1c)) and the traditional spacing disk type (Fig. 1d)) are designed and fabricated for experimental validation of the proposed approach.

B. Constant-Curvature-Based Kinematic Modeling

The constant-curvature approximation has been commonly applied to derive the kinematic model of various continuum manipulators. It forms an analytical closed-form relationship between the proximal actuation inputs and the distal tip position output and benefits the real-time control due to its simplification. According to this approximation, the elastic bending of a cable-driven continuum manipulator can be described by two mappings, as shown in Fig. 2a). The first mapping utilizes the variable of cable lengths $\boldsymbol{u} = [l_1, l_2, l_3, l_4]^T$, i.e., from the actuator space to describe constant-curvature arcs in the configuration space. Such information will be further mapped and derived to the distal tip position information $\boldsymbol{p} = [x, y, z]^T$ in the task space. These two mappings are described by manipulator-specific kinematics $g: u \mapsto q$, and manipulator-independent kinematics $h: \boldsymbol{q} \mapsto \boldsymbol{p}$, respectively. Hence, the complete kinematic mapping that computes the distal tip position depending on the cable lengths can be given by $f = h(g(\cdot))$.

All the coordination frames concerning a single-section continuum manipulator (Fig. 2b)) are described below, which are the base coordinate frame $O_b\{x_b y_b z_b\}$ and the distal tip coordinate frame $O_e\{x_e y_e z_e\}$, respectively. As a result, the position vector of the distal tip point expressed in the base coordinate frame can be obtained.

$$\boldsymbol{p} = \begin{bmatrix} x \\ y \\ z \end{bmatrix} = \begin{bmatrix} \frac{s}{\theta}\cos\varphi(1-\cos\theta) \\ \frac{s}{\theta}\sin\varphi(1-\cos\theta) \\ s\frac{\sin\theta}{\theta} \end{bmatrix} \tag{1}$$

Equation (1) could be utilized to solve the position of the distal tip with respect to the arc parameters. These arc parameters could be controlled by tuning the lengths of the cables. Therefore, it is necessary to derive the mapping relationship from the proximal actuation inputs (cable lengths) to the arc parameters as below.

$$s(\boldsymbol{u}) = \frac{l_1 + l_2 + l_3 + l_4}{4} \tag{2}$$

$$\theta(\boldsymbol{u}) = \frac{(l_1 - 3l_2 + l_3 + l_4)\sqrt{(l_4 - l_2)^2 + (l_3 - l_1)^2}}{4r(l_4 - l_2)} \tag{3}$$

$$\varphi(\boldsymbol{u}) = \arctan\left(\frac{l_3 - l_1}{l_2 - l_4}\right) \tag{4}$$

For the actuator space, the kinematic control could be approximated by enforcing equal and opposite cable displacement of the antagonistic pairs $[(l_1, l_3), (l_2, l_4)]$. This approximation assumes inextensible cables and an incompressible continuum body after the initial tensioning. As a result, the vector of $\boldsymbol{u}$ could be simplified as $[l_1, l_2]^T$. For the task space, the vector of $\boldsymbol{p}$ ($[x, y, z]^T$) in (1) could also be simplified as $[x, y]^T$, because the value of z can be computed from the values of x and y. Hereby, the closed-form forward kinematics is derived for the designed cable-driven continuum manipulators.

A Jacobian matrix $\boldsymbol{J}(\boldsymbol{u})$ is a multi-dimensional form of partial derivatives with respect to time for the forward kinematics (5), which reveals the velocity-level relationship (6) below.

$$\boldsymbol{p} = f(\boldsymbol{u}) = h\big(g(\boldsymbol{u})\big) \tag{5}$$

$$\dot{\boldsymbol{p}} = \frac{\partial f}{\partial \boldsymbol{u}}\dot{\boldsymbol{u}} = \frac{\partial h}{\partial g}\frac{\partial g}{\partial \boldsymbol{u}}\dot{\boldsymbol{u}} \tag{6}$$

$$\boldsymbol{J}(\boldsymbol{u}) = \frac{\partial h}{\partial g}\frac{\partial g}{\partial \boldsymbol{u}} \tag{7}$$

$$\begin{bmatrix}\Delta x\\ \Delta y\end{bmatrix} = \boldsymbol{J}(\boldsymbol{u})\begin{bmatrix}\Delta l_1\\ \Delta l_2\end{bmatrix} \quad (8)$$

where $\boldsymbol{J}(\boldsymbol{u})$ denotes a time-varying 2×2 matrix whose elements are nonlinear functions of the instant actuator states expressed by $\boldsymbol{u}$. The mapping relationship $J(\boldsymbol{u})$ represents a highly nonlinear and time-varying function that contains uncertainties caused by actuator hysteresis, frictions, and external loadings during practical applications. However, the Jacobian matrix based on the kinematic model cannot take the above uncertainties into account. Thus, it is difficult to be precisely obtained in either analytical or numerical ways.

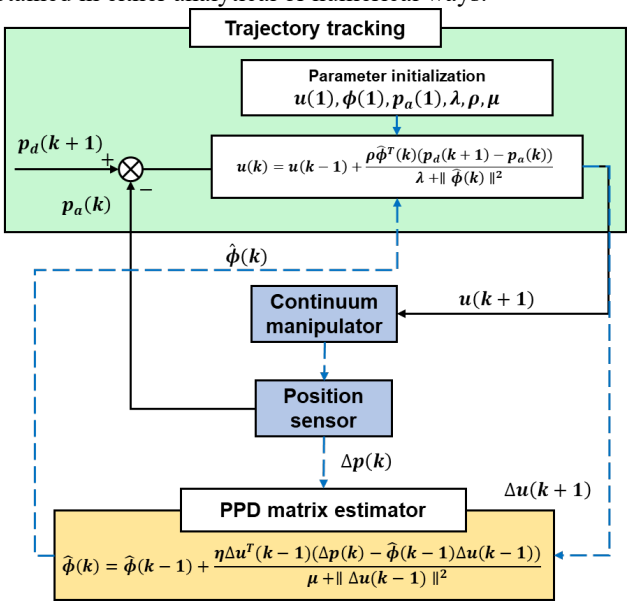

Fig. 3. The framework of the proposed MFAC controller.

C. The MFAC-Based Control Framework

This section presents an online model-free adaptive controller that utilizes the MFAC-based algorithm to address the inaccuracy and instability associated with the above model-based approach and overcome the uncertainties and nonlinearities of continuum manipulators. The framework of the presented MFAC controller has been illustrated in Fig. 3. The control algorithm needs to discretize and dynamically linearize the motion process of the continuum actuator with unknown and nonlinear factors and finally obtain the DLD model as below:

$$\Delta\boldsymbol{p}(k+1) = \phi(k)\Delta\boldsymbol{u}(k) \quad (9)$$

where $\Delta\boldsymbol{p}$ represents the change of the distal tip position of the continuum manipulator, $\Delta\boldsymbol{u}$ denotes the change of the cables, $\boldsymbol{\phi}(k)$ is the PPD matrix. The PPD matrix is updated based on the I/O measurement data of the continuum manipulator moving process. In each control loop, the updated PPD matrix is substituted into the control law to complete the motion control of the continuum manipulator.

The DLD model can effectively simplify the nonlinear model, and reduce the difficulty of control, so as to improve the real-time performance of online control. The time-varying PPD could be updated merely using the I/O measurement data of the controlled continuum manipulator, which help the controller adapt to different motion states and the design of continuum manipulators.

1) *Kinematics discretization and linearization to the DLD model*

For applying the MFAC-based control scheme, the continuum manipulator's continuous-time kinematics model will be first transformed into a DLD model. In this process, the kinematics of the continuum manipulator could be regarded as a multiple-input and multiple-output (MIMO) nonlinear discrete-time system [31], as expressed below.

$$\boldsymbol{p}(k+1) = \mathcal{F}\left(\boldsymbol{p}(k), \dots, \boldsymbol{p}(k-n_p), \boldsymbol{u}(k), \dots, \boldsymbol{u}(k-n_u)\right) \quad (10)$$

where $\boldsymbol{p}(k) \in R^2$ and $\boldsymbol{u}(k) \in R^2$ represent the system outputs (distal tip position values) and the control inputs (cable lengths), respectively. n_p and n_u are the unknown orders, and $\mathcal{F}(\cdot)$ denotes an unknown nonlinear function.

According to the kinematic model of the continuum manipulator presented in the last section, the partial derivatives of $\mathcal{F}(\cdot)$ in function (10) with respect to the control inputs $\boldsymbol{u}(k)$ are continuous. Furthermore, the single-section continuum manipulator satisfies the generalized *Lipschitz* condition, because the distal tip position change rates (output) cannot go to infinity if the change of the cable lengths (input) is at a finite altitude. This condition limits the rates of changes in the system outputs driven by the changes in the control inputs. Therefore, for each fixed k and $\|\boldsymbol{u}(k)\| \neq 0$, there exists $\|\Delta\boldsymbol{p}(k+1)\| \leq b\|\Delta\boldsymbol{u}(k)\|$.

Based on these two conditions, for each fixed k, there exists a time-varying PPD matrix $\boldsymbol{\phi}(k)$, such that nonlinear function (10) could be transformed into the proposed equivalent DLD model (9), where $\boldsymbol{\phi}(k) = \begin{bmatrix}\phi_{11}(k) & \phi_{12}(k)\\ \phi_{21}(k) & \phi_{22}(k)\end{bmatrix}, \|\boldsymbol{\phi}(k)\| \leq b$ and b is a positive constant [31]. The PPD matrix's existence has already been validated and guaranteed by rigorous mathematical analysis based on the differential mean value theorem [31]. This equivalent DLD model is derived only based on the I/O measurement data during the continuum manipulator movement, and no dynamic model is needed. It can be preliminarily expanded as below.

$$\begin{aligned}\begin{bmatrix}\Delta x\\ \Delta y\end{bmatrix} &= \begin{bmatrix}\phi_{11}(k) & \phi_{12}(k)\\ \phi_{21}(k) & \phi_{22}(k)\end{bmatrix}\begin{bmatrix}\Delta l_1\\ \Delta l_2\end{bmatrix}\\ &= \begin{bmatrix}\Delta l_1\phi_{11}(k) + \Delta l_2\phi_{12}(k)\\ \Delta l_1\phi_{21}(k) + \Delta l_2\phi_{22}(k)\end{bmatrix}\end{aligned} \quad (11)$$

As shown in Fig. 2b), a pair of antagonistic cables l_1 and l_3 mainly controls the movement in the x direction and has negligible influence in the y direction. This works the same for l_2 and l_4. Therefore, Δl_1 and Δl_2 can generate critical influences on Δx and Δy, respectively. As a result, $\boldsymbol{\phi}(k)$ is a diagonally dominant matrix and meets the following constraints, i.e., $|\phi_{ij}(k)| \leq b_1$, $b_2 \leq |\phi_{ii}(k)| \leq ab_2$, $i = 1,2$, $j = 1,2$, $i \neq j$, $a \geq 1$, $b_2 > 2b_1(2a+1)$ [32].

2) *The control law of the MFAC-based control framework*

The detailed control law of the presented MFAC-based control framework is derived for the continuum manipulator to achieve trajectory tracking. The criterion function of control inputs has been designed as follows.

$$I(\boldsymbol{u}(k)) = \|\boldsymbol{p}_d(k+1) - \boldsymbol{p}_a(k+1)\|^2 + \lambda \| \boldsymbol{u}(k) - \boldsymbol{u}(k-1) \|^2 \quad (12)$$

where $\boldsymbol{p}_d(k+1)$ denotes the desired distal tip position and λ is a weighting constant. This criterion has been designed to ensure the minimum difference between the desired position $\boldsymbol{p}_d$ of the controller and the actual position $\boldsymbol{p}_a$, and the minimum difference between the inputs at the two adjacent moments. Therefore, the control accuracy and smooth movement can be guaranteed.

By substituting the DLD model (9) into the criterion function (12), the new function will be differentiated with respect to $\boldsymbol{u}(k)$. Then setting it as zero, the MFAC control law can be derived as follows.

$$\boldsymbol{u}(k) = \boldsymbol{u}(k-1) + \frac{\rho \hat{\boldsymbol{\phi}}^T(k)\left(\boldsymbol{p}_d(k+1) - \boldsymbol{p}_a(k)\right)}{\lambda + \| \hat{\boldsymbol{\phi}}(k) \|^2} \quad (13)$$

where ρ is a step-size constant, and it is introduced to make this control law more general. Another parameter λ has also been introduced to serve as a penalty factor for $\| \Delta\boldsymbol{u}(k) \|$ and a constraint to suppress $\hat{\boldsymbol{\phi}}(k)$ from changing frequently. The bounded-input bounded-output (BIBO) stability of the closed-loop controller could be proved and guaranteed since the PPD matrix $\boldsymbol{\phi}(k)$ is a diagonally dominant matrix. The detailed derivation of the stability of the MFAC controller has been effectively analyzed based on the BIBO stability theory and the Gershgorin disc theorem [31]. Due to the lengthy derivation process, the corresponding contents have been added in the supporting document of part A in Appendix. The similar derivation process and relative conclusion have been previously performed and proved in [31], [32].

3) *Online estimation of the PPD matrix by the modified projection algorithm*

A time-varying algorithm, term as the modified projection algorithm, is utilized to realize an online estimation of the PPD matrix $\boldsymbol{\phi}(k)$ [31]. A criterion function of the PPD estimation is given below.

$$I(\boldsymbol{\phi}(k)) = \|\Delta\boldsymbol{p}(k) - \boldsymbol{\phi}(k)\Delta\boldsymbol{u}(k-1)\|^2 + \mu\left\|\boldsymbol{\phi}(k) - \hat{\boldsymbol{\phi}}(k)\right\|^2 \quad (14)$$

where $\mu > 0$ denotes a penalty factor on $\left\|\Delta\hat{\boldsymbol{\phi}}(k)\right\|$ and $\hat{\boldsymbol{\phi}}(k)$ represents the estimation value of $\boldsymbol{\phi}(k)$.

The criterion function is designed to ensure the minimum difference between the distal tip position changes and the minimum variation of the PPD matrix at two adjacent moments. This targets to avoid the vibration caused by the continuum manipulator motion's acceleration mutation and improve the PPD estimation's stability.

Substitute $\boldsymbol{\phi}(k) = \hat{\boldsymbol{\phi}}(k-1)$ into the criterion function (14), then differentiate it with respect to $\boldsymbol{\phi}(k)$ and consider it equal to zero. The PPD estimation could be obtained using the modified projection algorithm as below.

$$\hat{\boldsymbol{\phi}}(k) = \hat{\boldsymbol{\phi}}(k-1) + \frac{\eta\Delta\boldsymbol{u}^T(k-1)\left(\Delta\boldsymbol{p}(k) - \hat{\boldsymbol{\phi}}(k-1)\Delta\boldsymbol{u}(k-1)\right)}{\mu + \| \Delta\boldsymbol{u}(k-1) \|^2} \quad (15)$$

where η represents a step-size constant, and the role of η and μ in (15) are similar to that of ρ and λ in (13).

Given that the motion of the continuum manipulator can experience sudden changes, a reset algorithm is presented and applied to improve the stability of the time-varying trajectory tracking process and suppress the vibration of the continuum manipulator. The reset algorithm of $\hat{\boldsymbol{\phi}}(k)$ is defined as follows.

$$\begin{aligned} \hat{\phi}_{ii}(k) &= \hat{\phi}_{ii}(1), \text{if } \left|\hat{\phi}_{ii}(k)\right| < b_2 \text{ or } \left|\hat{\phi}_{ii}(k)\right| > \alpha b_2 \\ &\quad \text{or } \|\Delta\boldsymbol{u}(k-1)\| < err \text{ or } \left\|\hat{\boldsymbol{\phi}}(k)\right\| < err \\ \hat{\phi}_{ij}(k) &= \hat{\phi}_{ij}(1), \text{if } \left|\hat{\phi}_{ij}(k)\right| > b_1 \text{ or } \|\Delta\boldsymbol{u}(k-1)\| < err \\ &\quad \text{or } \left\|\hat{\boldsymbol{\phi}}(k)\right\| < err\ ,\ i \neq j \end{aligned} \quad (16)$$

where $\hat{\phi}_{ij}(0)$ represents the initial value of $\hat{\phi}_{ij}(k)$, $i = 1,2$, $j = 1,2$. err denotes the minimum limit of a matrix norm. When significant disturbances and uncertainties occur or there exist distortions in the sensor signals, the above-presented reset algorithm can rapidly rest the PPD matrix and eliminate the impacts on the controller made by the previous motion states, as well as improve the robustness of the PPD estimation.

The detailed parameter initialization is presented below. For the setting of $\hat{\boldsymbol{\phi}}(0)$, it should be noted that the control performance of the MFAC controller is sensitive to the value of $\hat{\boldsymbol{\phi}}(0)$, especially the sign of each element. Therefore, a straightforward setting method for $\boldsymbol{\phi}(k)$ based on physical interpretation is proposed. From the DLD model (9), $\boldsymbol{\phi}(k)$ describes a direct mapping from the variation of cable lengths $\Delta\boldsymbol{u}(k)$ to the variation of the distal tip position $\Delta p(k+1)$, which are in the same direction. In other words, u has a positive effect on p. Thus, $\hat{\boldsymbol{\phi}}(0)$ could be set as a positive diagonal matrix. The setting of a, b_1 and b_2 determines the range of PPD estimation, and they are also essential to the performance of PPD estimation. It is evident that the decrease in the range of PPD estimation, especially $\hat{\phi}_{ii}(k)$, will improve the robustness and adaptation of the algorithm for sudden changes in the system. However, if the range of $\hat{\phi}_{ii}(k)$ is selected to be small, then the number of reset times of $\hat{\boldsymbol{\phi}}(k)$ will increase significantly, deteriorating the tracking performances. As a result, there exist trade-offs among different design considerations. Meanwhile, to maintain the stability of the MFAC controller, the err is added to the reset algorithm as a novel constraint to reset the PPD matrix when it changes too much caused by variable and unknown external loadings. The constraint on the sign of PPD matrix parameters is also deleted from the traditional reset algorithm [31], which is more suitable for the highly nonlinear continuum robot system (Fig. A1 of part B in Appendix). The PPD matrix should not be reset frequently due to the normal parameter sign changes. Moreover, the step-size constant ρ, η and penalty factor λ, μ in the controller also need to be adjusted manually before the controller is applied.

It can be seen that the change of the PPD matrix parameters can be inherited by subsequent control loops and combined with the reset algorithm (16) to make the parameter estimation algorithm have a more vital ability to track time-varying parameters. The continuum robot's motion state changes dramatically at the initial interference stage. The reset algorithm can reset the PPD matrix, eliminate influences from the

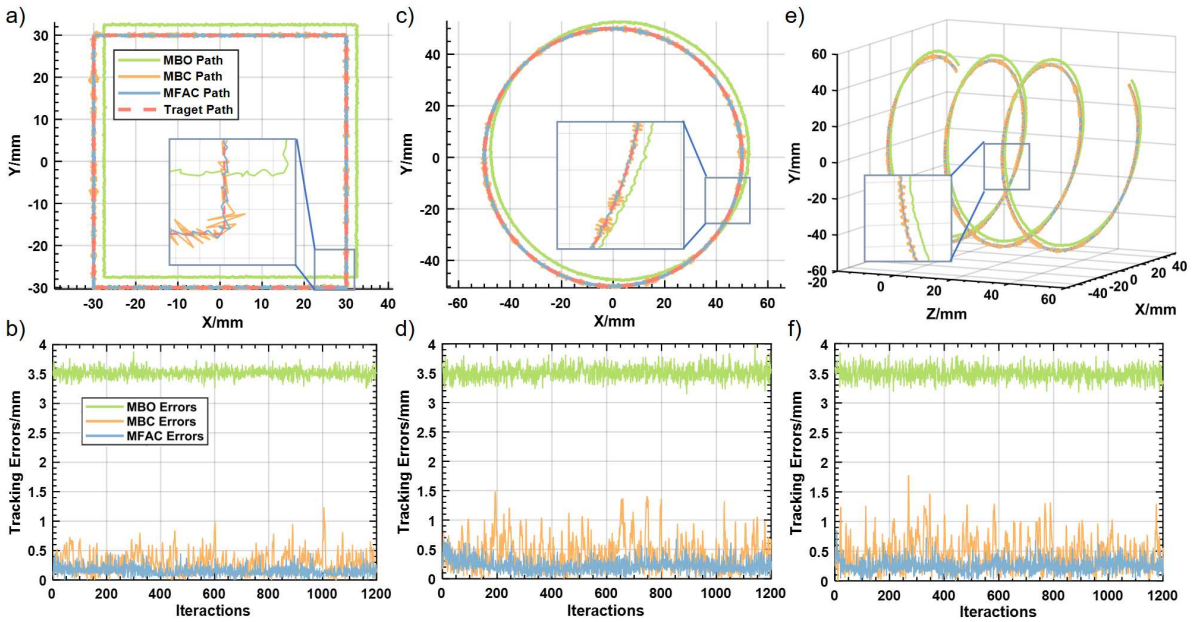

Fig. 4. The tracking performances and the tracking error variations for different position controllers on simulations. a)-b) The tracking performance and the tracking error variation on a rectangle path; c)-d) The tracking performance and the tracking error variation on a circle path; e)-f) The tracking performance and the tracking error variation on a spiral path.

previous motion states on the controller, and quickly adapt to the changed motion state. When the interference persists, the change of PPD matrix parameters will be retained in the subsequent control loops, making it return to the target path quickly. Meanwhile, the PPD matrix changed by the persistent disturbances can suppress the influence of these disturbances on the subsequent trajectory tracking. These advantages bring the controller high precision, strong robustness, and fast response to nonlinear and random disturbances. Moreover, the controller is constructed by solely utilizing the online I/O measurement data of the continuum manipulator and has no relation with any explicit model dynamics and structural information of the system. Therefore, the proposed MFAC control scheme is a typical model-free control framework, which gives this controller better transfer ability in controlling continuum manipulators with different configurations.

D. Simulations for Different Controllers on Trajectory Tracking of Three Predefined Paths

This section implements simulations of the proposed MFAC controller in MATLAB R2019a to investigate its feasibility and control performances. To compare with the proposed approach, two other typical position controllers for the continuum robots have also been conducted.

1) *Model-based open-loop controller*

The model-based open-loop controller (MBO) is established based on the constant-curvature kinematic model proposed in Section II.B. Since the model information of the continuum robot is already known, its Jacobian $\boldsymbol{J}^{\dagger}$can be directly calculated. Therefore, the tracking control could be solved as below:

$$\dot{\boldsymbol{u}}(k) = \boldsymbol{J}^{\dagger}(k)\,\dot{\boldsymbol{p}}_d(k) \tag{17}$$

where $\boldsymbol{p}_d$ denotes the desired path.

2) *Model-based closed-loop controller*

To correct the accumulated errors, the model-based open-loop controller (17) could be modified to form a model-based closed-loop controller (MBC) with distal position feedback.

$$\dot{\boldsymbol{u}}(k) = \boldsymbol{J}^{\dagger}(k)\left(\dot{\boldsymbol{p}}_d(k) + K_p\big(\boldsymbol{p}_d(k) - \boldsymbol{p}_a(k)\big)\right) \tag{18}$$

where $\boldsymbol{p}_a$ represents the actual feedback path, and K_p denotes the proportional parameter of the controller.

The accuracy and stability of these three controllers are investigated with three target paths of 2D rectangle and circle shapes and a 3D spiral shape. The direction of the Jacobian matrix and movement stay changed along these paths. Hence, it is an appropriate scenario to analyze the controller's performance, and the experimental configuration's simulation parameters are listed in Table I.

TABLE I
PARAMETERS OF THE SIMULATION CONFIGURATION

Parameters	Value
Length of the continuum robot	200 mm
Diameter of the continuum robot	20 mm
Side length of rectangle path	60 mm
Radius of the circular/spiral path	50 mm
Pitch the spiral path	6 mm
Total control intervals	1200

TABLE II
PARAMETERS OF THE MFAC CONTROLLER IN SIMULATIONS

Symbol	Value	Symbol	Value
$\boldsymbol{\phi_0}$	$\begin{bmatrix}5 & 1\\ 1 & 5\end{bmatrix}$	$\boldsymbol{\mu}$	0.34
$\boldsymbol{\lambda}$	0.5	$\boldsymbol{\eta}$	0.5
$\boldsymbol{\rho}$	1		

The white noise with a signal-to-noise ratio of 60 dB is introduced as the robot's random error during simulations. Three proposed controllers were evaluated under the same experimental setup. The K_p of the MBC controller is tuned as

1.8, and the parameters of the MFAC controller are enumerated in Table II. The tracking results for the target paths are illustrated in Fig. 4 and Table III. The dynamic changes of the PPD matrix are shown in Fig. A1 of part B in Appendix. The trajectory tracking errors on these three paths of MBO are significantly higher than that of MBC and MFAC. Because it is an open-loop controller without the distal tip position feedback, errors could accumulate during the task execution. Thus, the premise of this controller is to work under ideal conditions without external interferences, making it challenging to be applied in practical applications. The closed-loop controller MBC tackles the error accumulation problem and greatly improves the control accuracy, as illustrated by the error values in Table III. However, this method suffers from a large amount of calculation and produces noticeable variations on actual tracking paths (Fig. 4). Another significant problem these model-based controllers face is the non-negligible error caused by the deformation of continuum robots or the inaccuracy of model parameters. The proposed model-free MFAC controller is applied to solve the inaccurate modeling problem and further reduce the error, resulting in a more accurate and smoother tracking path. The overall mean errors of 0.20 mm (0.1% of its length) and maximum errors of 0.68 mm (0.34% of its length) are lower than that of MBC by 50% and 49%, respectively, demonstrating stability and high accuracy of the proposed controller. Under these circumstances, the superiorities of the MFAC controller are revealed and will be further demonstrated with experimental validation.

TABLE III
SIMULATION RESULTS OF DIFFERENT CONTROLLERS

Path	Method	Mean Error (mm)	Relative Mean Error	Max Error (mm)	Relative Max Error
Rectangle	MBO	3.52	1.76%	3.81	1.90%
	MBC	0.32	0.16%	1.12	0.56%
	MFAC	0.14	0.07%	0.44	0.22%
Circle	MBO	3.45	1.72%	3.86	1.93%
	MBC	0.45	0.22%	1.54	0.77%
	MFAC	0.21	0.10%	0.77	0.38%
Spiral	MBO	3.49	1.74%	3.89	1.94%
	MBC	0.42	0.21%	1.38	0.69%
	MFAC	0.26	0.13%	0.85	0.42%
Mean of Three Paths	MBO	3.49	1.74%	3.85	1.92%
	MBC	0.40	0.20%	1.35	0.68%
	MFAC	0.20	0.10%	0.69	0.34%

III. EXPERIMENTS AND RESULTS

A. Experiments Setup

The experimental configuration of the robotic control system has been built to validate the proposed MFAC controller, as illustrated in Fig. 5. This control system mainly consists of a motion controller (GOOGOLTECH, GTS-800, China), five driving amplifiers (IMC, PENP, Germany), a 3D optical measurement unit (NDI Polaris, Ontario, Canada), and the proposed continuum robot and a host computer (Core i7 processor @ 2.80 GHz, and 16-GB RAM). The motion controller sends commands to the amplifiers and drives DC motors to actuate the continuum robot. The 3D optical measurement unit measures the robot's distal tip position with the attached maker. The position data is sent to the host computer for position feedback with a sampling rate of 60 Hz through a USB cable.

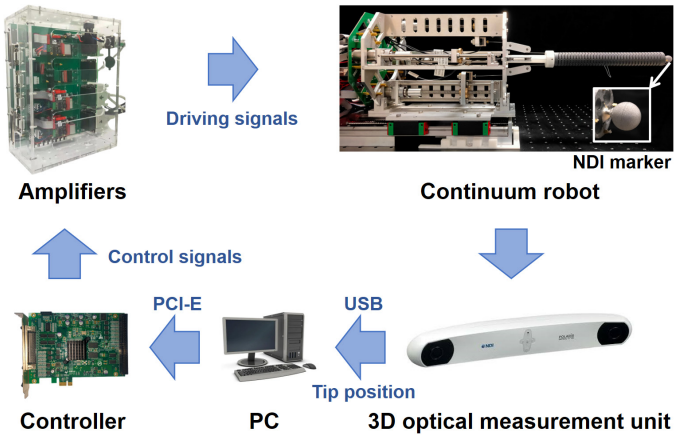

Fig. 5. The experimental configuration for the investigation of the presented controllers.

B. The Trajectory Tracking of Three Predefined Paths in the Free Space

TABLE IV
EXPERIMENTAL PARAMETERS OF THE MFAC CONTROLLER

Symbol	Value	Symbol	Value
$\boldsymbol{\phi_0}$	$\begin{bmatrix}5 & 1\\ 1 & 5\end{bmatrix}$	$\boldsymbol{\mu}$	2.3
$\boldsymbol{\lambda}$	0.6	$\boldsymbol{\eta}$	0.7
$\boldsymbol{\rho}$	0.4		

To evaluate the effectiveness of the MFAC controller for trajectory tracking, three groups of experiments were conducted with the three presented target paths in free space. The experimental configuration parameters were the same as the simulation, as shown in Table I. The K_p of the MBC controller was tuned as 0.4, and the parameters of the MFAC controller are enumerated in Table IV. The control frequency was set at about 20 Hz because data from different devices (such as amplifiers and the 3D optical measurement unit) needed to be synchronized to keep the controller stable.

TABLE V
EXPERIMENTAL RESULTS OF DIFFERENT CONTROLLERS IN FREE SPACE

Path	Method	Mean Error (mm)	Relative Mean Error	Max Error (mm)	Relative Max Error	Time Cost (s)
Rectangle	MBO	3.97	1.98%	8.18	4.09%	-
	MBC	1.42	0.71%	3.39	1.70%	67
	MFAC	1.02	0.51%	2.38	1.19%	62
Circle	MBO	7.36	3.68%	9.40	4.70%	-
	MBC	1.72	0.86%	3.86	1.93%	76
	MFAC	1.17	0.58%	2.75	1.38%	70
Spiral	MBO	9.46	4.73%	17.85	8.92%	-
	MBC	4.23	2.12%	7.90	3.95%	178
	MFAC	3.28	1.64%	5.20	2.60%	162
Mean of Three Paths	MBO	6.93	3.46%	11.81	5.90%	-
	MBC	2.46	1.23%	5.05	2.52%	107
	MFAC	1.82	0.91%	3.44	1.72%	98

The tracking results for different target paths are illustrated in Fig. 6, and the quantitative tracking errors in terms of mean and maximum errors are listed in Table V. MBO generated a

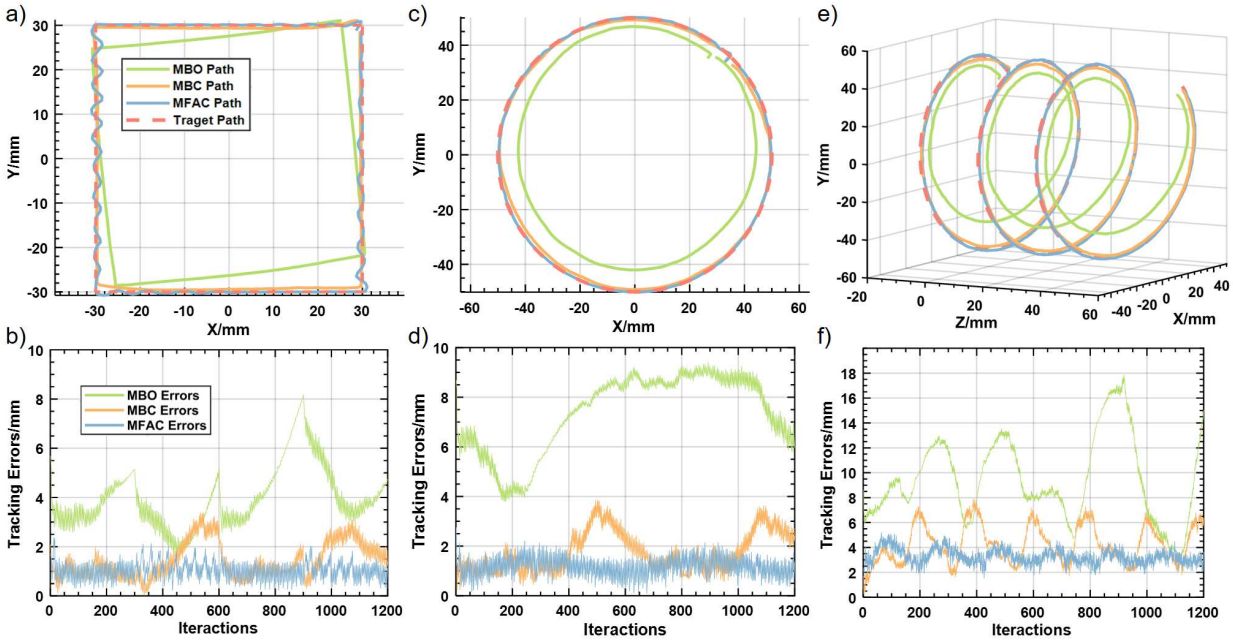

Fig. 6. The tracking performances and the tracking error variations for different position controllers on experiments. a)-b) The tracking performance and the tracking error variation on a rectangle path; c)-d) The tracking performance and the tracking error variation on a circle path; e)-f) The tracking performance and the tracking error variation on a spiral path.

large mean error of 6.93 mm for the three trajectory paths due to the open control strategy. MBC significantly reduced the error to 2.46 mm based on the distal end position feedback. Compared with these two controllers, the proposed MFAC controller can achieve smooth tracking results with lower errors. The corresponding mean error of 1.82 mm (0.91% of its length) and maximum errors of 3.44 mm (1.72% of its length) were lower than that of MBC by 26% and 32%, respectively. The MFAC controller still retains the high accuracy of the model-free controller in actual experiments. Furthermore, the MFAC controller takes an average of 98 s in three trajectory tracking experiments and reduces the time cost by 8.4% compared with the traditional MBC controller (107 s). Such results indicate that the proposed MFAC controller has a lower computational cost. The tracking error of the spiral path was larger than that of the circular path. Because the spiral path requires completing three circles of circular motion in the same 1200 iterations (Table I), the number of iterations per circle was only one-third of that of the circular path. The fewer number of iterations increased the errors of these controllers.

C. The Trajectory Tracking under Variable Disturbances

The trajectory tracking experiments with variable external disturbances/loading have been performed to further verify the robustness and response speed of the presented MFAC controller. The parameters of experiment configuration and controllers remain the same, as enumerated in Tables I and IV. The first two experiments (Exp. 1-2) changed the loading's weight and the location by successively adding two standard weights of 100 g and 50 g randomly at different locations along the vertical direction during the movement along the two target paths of the 2D rectangle and circle shapes (Fig. 7a)). The third experiment (Exp. 3) followed the 3D spiral path, loaded two weights of 100 g and 50 g, and unloaded the 100 g weight around each circular path apex. The fourth experiment (Exp. 4) generated disturbances along the radial direction using a pulley and repeated the steps of the third experiment but unloaded the 50 g weight for easy operation (Fig. 7b)).

The tracking results for three target paths are illustrated in Fig. 7 and Table VI. The results of the MBO controller are not shown in the figures because its corresponding errors are too large to display. The influences of variable loadings on tracking motions are pronounced. Thus, two indicators that include the deviation of motion tracking (DMT) of the continuum robot distal tip and the number of iterative steps (NIS) to compensate for these deviations have been defined, as labeled in Fig. 7g), to reflect the influences under variable loadings. They can indicate control accuracy, response speed, and robustness of the control algorithm.

In the first three groups of experiments, the overall mean error (1.86 mm, 0.93% of its length) of the MFAC controller was 25% less than that of the MBC controller, as shown in Table VI. When the loading changed, the DMT values of the MFAC controller were obviously smaller than that of the MBC controller. The average number of the NIS required by the MFAC controller for 100 g and 50 g were 17 steps and 10 steps, respectively. They were 77% and 73% less than the MBC controller. These results demonstrated that the MFAC controller responds more quickly to variable loading. For the fourth group of experiments, it was challenging for the controller to track the spiral path and compensate for the variable loading, as indicated by the path profile in Fig. 7f). The MFAC controller achieved a more smooth and close path profile to the target path. Its mean error was 3.47 mm (1.74% of its length), which was 49% less than that of the MBC controller. In this case, the radial loading direction was constantly changing due to the used pulley, thus requiring the control algorithm to have a faster response speed and stronger

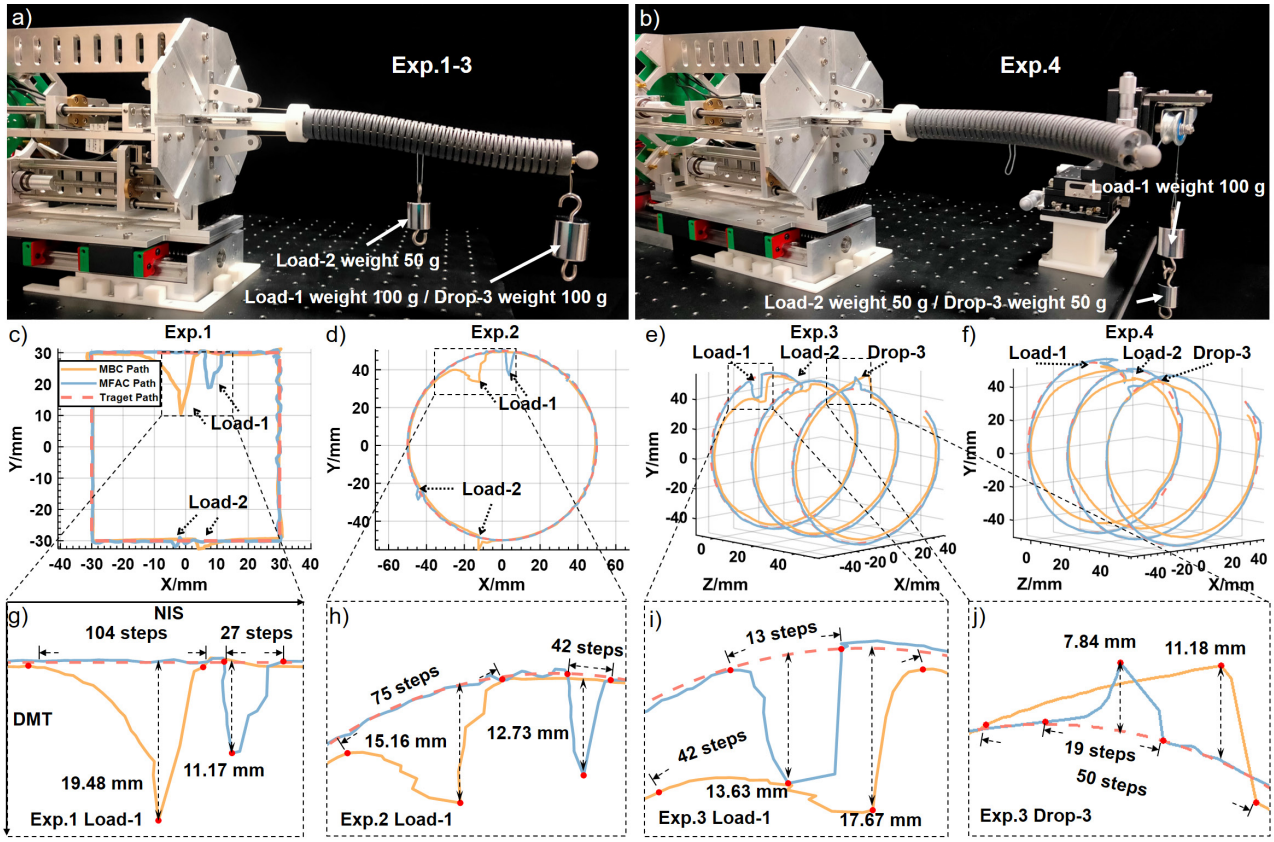

Fig. 7. a) The experimental configuration for Exp.1-3; b) The experimental configuration for Exp.4; c)-f) The tracking performances for different controllers on Exp.1-4. g)-j) The DMT and NIS of the Exp.1 Load-1, Exp.2 Load-1, Exp.3 Load-1, and Exp.1 Drop-3.

TABLE VI
EXPERIMENTAL RESULTS OF DIFFERENT CONTROLLERS UNDER VARIABLE DISTURBANCES ON EXP.1-4

Method	Path	Mean Error (mm)	Relative Mean Error	Load-1 DMT (mm)	Load-2 DMT (mm)	Drop-3 DMT (mm)	Load-1 NIS	Load-2 NIS	Drop-3 NIS
MBC	**Exp.1**	1.59	0.80%	19.48	2.57		104	41	
MFAC	**Rectangle**	1.11	0.56%	11.17	1.91		27	13	
MBC	**Exp.2**	1.71	0.86%	15.16	7.43		75	42	
MFAC	**Circle**	1.09	0.54%	12.73	5.42		11	8	
MBC	**Exp.3**	4.16	2.08%	17.67	6.25	11.18	42	27	50
MFAC	**Spiral**	3.39	1.70%	13.63	3.74	7.84	13	9	19
MBC	**Exp.4**	6.79	3.40%						
MFAC	**Spiral**	3.47	1.74%						
MBC	**Mean error**	3.56	1.78%						
MFAC	**of Exp.1-4**	2.27	1.14%						

tracking ability. The MFAC controller still maintained excellent spiral trajectory tracking ability and compensation ability of continuously variable loadings.

D. The Transferability of the Proposed MFAC Controller on the other Continuum Manipulator

The same experiments were carried out on the other designed continuum manipulator with a central bone and discrete spacing disks without tuning any controller parameters to further verify the proposed MFAC controller's transferability. This manipulator shares the same length and diameter with the notched one and possesses a lower stiffness, resulting in poorer dynamic performances. Therefore, it is expected that the three controllers could generate larger mean errors than the previous experiments on the notched manipulator.

The tracking results for the three target paths in the free space are illustrated in Fig. 8 and Table VII. The MBO and MBC controllers produced larger errors than the previous experiments. Compared with these two controllers, the presented MFAC controller achieved smooth tracking results and the lowest mean error of 1.84 mm, which was almost the same as that of the notched continuum manipulator experiments. The experimental results of trajectory tracking under the variable disturbances have been displayed in Fig. 9 and Table VIII. The tracking error values of the MBC and MFAC controller have been increased to different degrees due to the lower stiffness and poorer dynamics of this continuum manipulator. The overall mean error of Exp. 1-4 (2.35 mm, 1.18% of its length) of the MFAC controller was only 3.5% larger than that of the notched continuum manipulator. However, the MBC controller produced a significant decrease in tracking performance, and the overall mean error of Exp. 1-4 (5.21 mm,

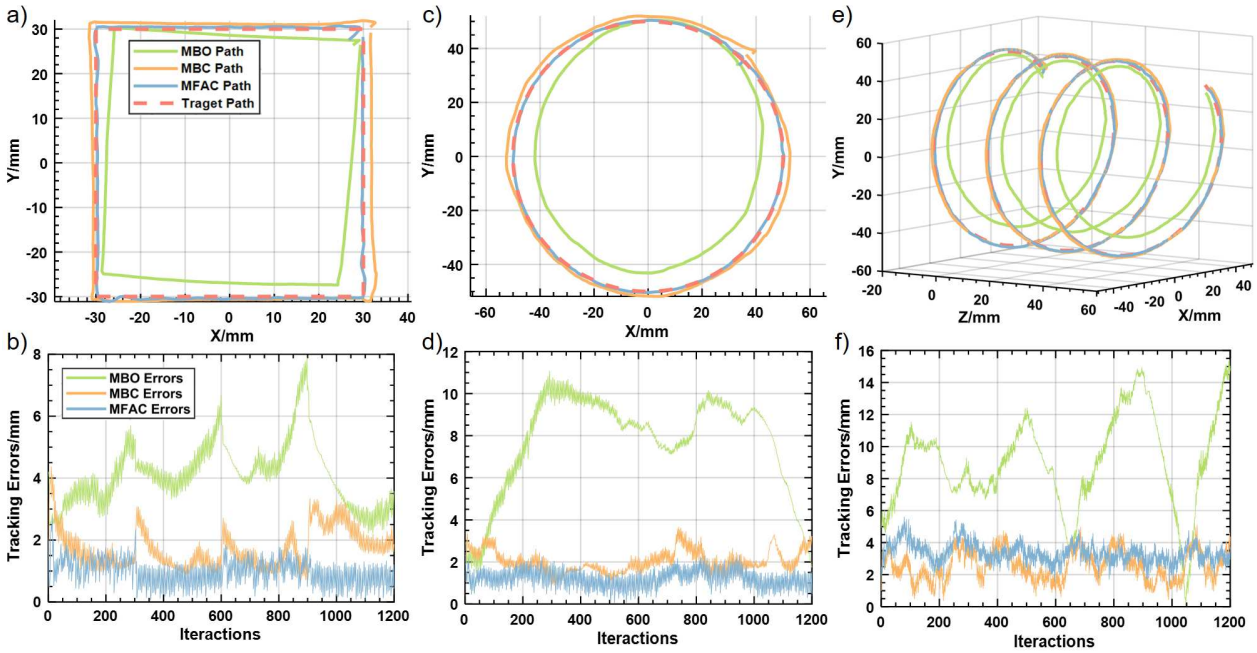

Fig. 8. The tracking performances and the tracking error variations for different position controllers on experiments. a)-b) The tracking performance and the tracking error variation on a rectangle path; c)-d) The tracking performance and the tracking error variation on a circle path; e)-f) The tracking performance and the tracking error variation on a spiral path.

TABLE VII
EXPERIMENTAL RESULTS OF DIFFERENT CONTROLLERS IN FREE SPACE

Path	Method	Mean Error (mm)	Relative Mean Error	Max Error (mm)	Relative Max Error
Rectangle	MBO	4.12	2.06%	7.89	3.94%
	MBC	1.67	0.84%	4.37	2.18%
	MFAC	0.96	0.48%	2.73	1.36%
Circle	MBO	7.69	3.84%	11.06	5.53%
	MBC	2.02	1.01%	3.65	1.82%
	MFAC	1.21	0.60%	2.32	1.16%
Spiral	MBO	9.59	4.80%	15.72	7.86%
	MBC	4.52	2.26%	7.18	3.59%
	MFAC	3.36	1.68%	5.61	2.80%
Mean of Three Paths	MBO	7.13	3.56%	11.56	5.78%
	MBC	2.74	1.37%	5.06	2.53%
	MFAC	1.84	0.92%	3.55	1.78%

2.60% of its length) was 46.3% larger than before. After replacing the continuum manipulator, for experiments in the free space and with variable disturbances, the error of the MFAC controller only increased slightly and basically remained stable, but the error of the MBC controller increased much more significantly. These results demonstrated that the MFAC controller has better transferability than the MBC controller. The MFAC controller can maintain strong robustness when the bending stiffness of the continuum manipulator decreases by 50%.

E. Discussion

Although the simulations and experiments adopt the same desired paths, the errors of all experimental results are higher than those obtained by simulations. This happens because the continuum manipulators have uncertainties, such as manufacturing errors, friction, gravity, and vibration in motion, which are not considered in the simulated model. Meanwhile, the simulation cannot reflect the influence of different paths and continuum designs on the controller's precision.

When disturbances exist in the continuum manipulator motion process, the MFAC controller shows high robustness and tracking performance and can quickly return to the target path, as indicated in Figs. 7, 9 and Tables VI, VIII. The experiments of trajectory tracking under variable disturbances for two kinds of manipulators have demonstrated the advantages of the presented MFAC controller over the other controllers in terms of the mean error, DMT, and NIS. Especially when the disturbance is time-varying, the performance of the MFAC controller is significantly better than that of MBC. For the fourth experiment with variable radial loading, the presented MFAC controller well followed the spiral path with relatively small errors; however, the path generated by the MBF controller produced a significant deviation from the desired path with larger errors. Because the PPD matrix is updated through the I/O data, the matrix change can be reserved for subsequent control loops so that the MFAC controller can quickly adapt to the motion state when the disturbance persists. Moreover, the reset algorithm can recognize the sudden change of motion state, enhance the controller's stability, and help the controller achieve a fast response when the continuum manipulator is disturbed. In the experiments to verify the transferability of the different controllers, the continuum manipulator with smaller stiffness brings more errors to the model-based controllers. This is because the controllers based on the kinematic model cannot take the changes of the dynamic model into account. However, the MFAC controller only considers the relationship between the input and output of the system and can take into account the uncertainty and nonlinear factors in motion more comprehensively, which effectively enhances its transferability.

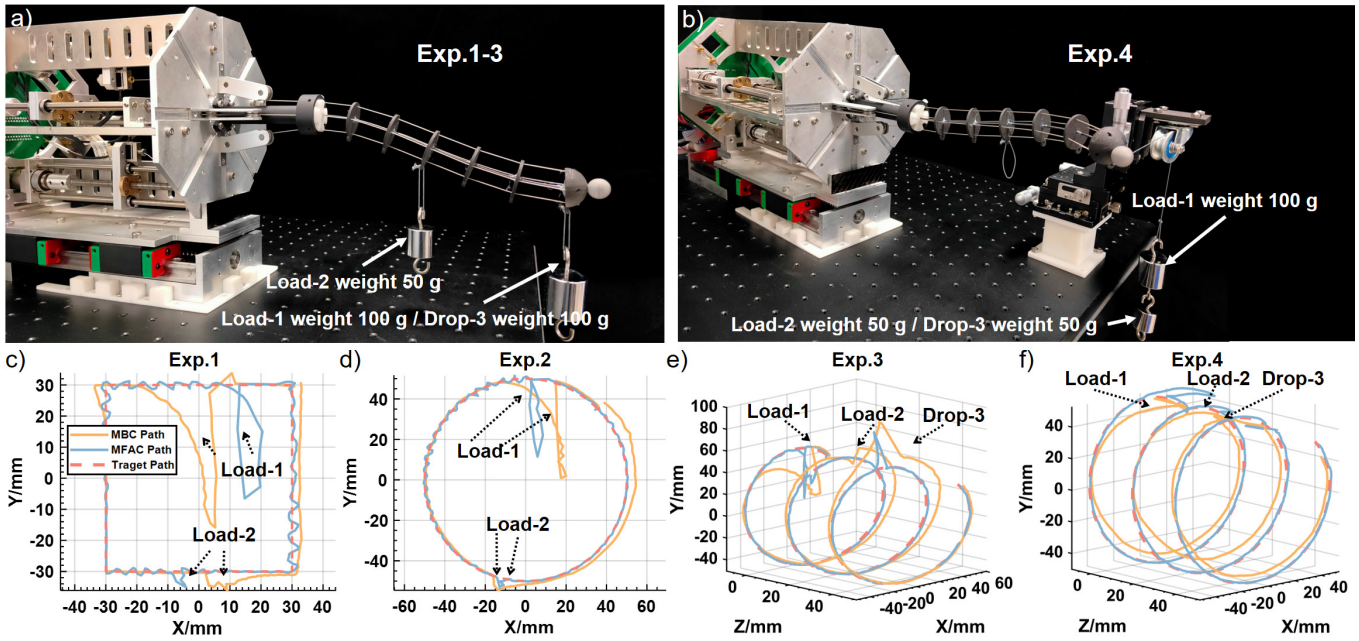

Fig. 9. a) The experimental configuration for Exp.1-3; b) The experimental configuration for Exp.4; c)-f) The tracking performances for different controllers on Exp.1-4.

TABLE VIII
EXPERIMENTAL RESULTS OF DIFFERENT CONTROLLERS UNDER VARIABLE DISTURBANCES ON EXP.1-4

Method	Path	Mean Error (mm)	Relative Mean Error	Load-1 DMT (mm)	Load-2 DMT (mm)	Drop-3 DMT (mm)	Load-1 NIS	Load-2 NIS	Drop-3 NIS
MBC	**Exp.1**	2.93	1.47%	45.84	6.08		153	113	
MFAC	**Rectangle**	1.34	0.67%	36.51	5.06		23	21	
MBC	**Exp.2**	3.52	1.76%	46.88	6.54		95	77	
MFAC	**Circle**	1.32	0.66%	38.18	5.04		20	22	
MBC	**Exp.3**	7.07	3.54%	42.21	5.22	40.19	65	12	55
MFAC	**Spiral**	3.08	1.54%	35.61	9.51	34.72	13	10	15
MBC	**Exp.4**	7.34	3.67%						
MFAC	**Spiral**	3.65	1.83%						
MBC	**Mean error**	5.21	2.61%						
MFAC	**of Exp.1-4**	2.35	1.18%						

IV. CONCLUSION

An online MFAC controller was proposed to realize continuum manipulators' precise and robust trajectory tracking control. Unlike the previous model-based methods that require an accurate mathematical model of the robotic system, the presented method employs the MFAC algorithm to estimate the real-time PPD matrix, overcoming the model complexities and uncertainty issues. The feasibility and superior performance of the presented control scheme were validated through both simulations and experiments. The experimental results show that the presented MFAC controller performs better under normal conditions and demonstrates excellent anti-disturbance ability and robustness against variable external loadings. Moreover, the MFAC controller shows excellent transferability in controlling different types of continuum manipulators. This current MFAC controller is mainly implemented based on kinematics, and it needs to be further improved by combining the dynamic model and multimodal sensing modalities to cope with high-speed variable disturbances. The dynamic model of the continuum manipulator can be derived based on Lagrange's equation and added to the online estimation algorithm of the PPD matrix. The fiber Bragg grating (FBG)-based sensing techniques [5], [33], [34] will be introduced into this control strategy to achieve shape and force feedback of the continuum manipulators. These sensing modalities can aid in parameter determination for the dynamics model. Furthermore, multi-section continuum manipulators with more degrees of freedom will also be analyzed and controlled with the MFAC-based approach.

REFERENCES

[1] J. Kim, M. de Mathelin, K. Ikuta, and D.-S. Kwon, "Advancement of Flexible Robot Technologies for Endoluminal Surgeries," *Proc. IEEE*, vol. 110, no. 7, pp. 909–931, Jul. 2022, doi: 10.1109/JPROC.2022.3170109.

[2] J. Zhu *et al.*, "Intelligent Soft Surgical Robots for Next-Generation Minimally Invasive Surgery," *Advanced Intelligent Systems*, vol. 3, no. 5, p. 2100011, May 2021, doi: 10.1002/aisy.202100011.

[3] P. Valdastri, M. Simi, and R. J. Webster, "Advanced Technologies for Gastrointestinal Endoscopy," *Annu. Rev. Biomed. Eng.*, vol. 14, no. 1, pp. 397–429, Aug. 2012, doi: 10.1146/annurev-bioeng-071811-150006.

[4] V. Vitiello, Su-Lin Lee, T. P. Cundy, and Guang-Zhong Yang, "Emerging Robotic Platforms for Minimally Invasive Surgery," *IEEE Rev. Biomed. Eng.*, vol. 6, pp. 111–126, 2013, doi: 10.1109/RBME.2012.2236311.

[5] C. Shi *et al.*, "Shape Sensing Techniques for Continuum Robots in Minimally Invasive Surgery: A Survey," *IEEE Trans. Biomed. Eng.*, vol. 64, no. 8, pp. 1665–1678, Aug. 2017, doi: 10.1109/TBME.2016.2622361.

[6] C. Bergeles and Guang-Zhong Yang, "From Passive Tool Holders to Microsurgeons: Safer, Smaller, Smarter Surgical Robots," *IEEE Trans. Biomed. Eng.*, vol. 61, no. 5, pp. 1565–1576, May 2014, doi: 10.1109/TBME.2013.2293815.

[7] Y. Song, S. Wang, X. Luo, and C. Shi, "Design and Optimization of a 3D Printed Distal Flexible Joint for Endoscopic Surgery," *IEEE Trans. Med. Robot. Bionics*, vol. 4, no. 1, pp. 38–49, Feb. 2022, doi: 10.1109/TMRB.2022.3142516.

[8] J. Troccaz, G. Dagnino, and G.-Z. Yang, "Frontiers of Medical Robotics: From Concept to Systems to Clinical Translation," *Annu. Rev. Biomed. Eng.*, vol. 21, no. 1, pp. 193–218, Jun. 2019, doi: 10.1146/annurev-bioeng-060418-052502.

[9] G. Tay, H.-K. Tan, T. K. Nguyen, S. J. Phee, and N. G. Iyer, "Use of the EndoMaster robot-assisted surgical system in transoral robotic surgery: A cadaveric study," *Int J Med Robotics Comput Assist Surg*, vol. 14, no. 4, p. e1930, Aug. 2018, doi: 10.1002/rcs.1930.

[10] M. Hwang and D. Kwon, "K-FLEX: A flexible robotic platform for scar-free endoscopic surgery," *Int J Med Robot*, vol. 16, no. 2, Apr. 2020, doi: 10.1002/rcs.2078.

[11] D. I. K. Fielding *et al.*, "First Human Use of a New Robotic-Assisted Fiber Optic Sensing Navigation System for Small Peripheral Pulmonary Nodules," *Respiration*, vol. 98, no. 2, pp. 142–150, 2019, doi: 10.1159/000498951.

[12] J. Burgner-Kahrs, D. C. Rucker, and H. Choset, "Continuum Robots for Medical Applications: A Survey," *IEEE Trans. Robot.*, vol. 31, no. 6, pp. 1261–1280, Dec. 2015, doi: 10.1109/TRO.2015.2489500.

[13] X. Luo, D. Song, Z. Zhang, S. Wang, and C. Shi, "A Novel Distal Hybrid Pneumatic/Cable-Driven Continuum Joint with Variable Stiffness Capacity for Flexible Gastrointestinal Endoscopy," *Advanced Intelligent Systems*, p. 2200403, Mar. 2023, doi: 10.1002/aisy.202200403.

[14] T. da Veiga *et al.*, "Challenges of continuum robots in clinical context: a review," *Prog. Biomed. Eng.*, vol. 2, no. 3, p. 032003, Aug. 2020, doi: 10.1088/2516-1091/ab9f41.

[15] Z. Zhang, G. Zhang, S. Wang, and C. Shi, "Hysteresis Modelling and Compensation for Tendon-Sheath Mechanisms in Robot-Assisted Endoscopic Surgery Based on the Modified Bouc-Wen Model with Decoupled Model Parameters," *IEEE Trans. Med. Robot. Bionics*, pp. 1–1, 2023, doi: 10.1109/TMRB.2023.3249234.

[16] P. E. Dupont, N. Simaan, H. Choset, and C. Rucker, "Continuum Robots for Medical Interventions," *Proc. IEEE*, vol. 110, no. 7, pp. 847–870, Jul. 2022, doi: 10.1109/JPROC.2022.3141338.

[17] G. J. Vrooijink, A. Denasi, J. G. Grandjean, and S. Misra, "Model predictive control of a robotically actuated delivery sheath for beating heart compensation," *The International Journal of Robotics Research*, vol. 36, no. 2, pp. 193–209, Feb. 2017, doi: 10.1177/0278364917691113.

[18] A. Bajo and N. Simaan, "Hybrid motion/force control of multi-backbone continuum robots," *The International Journal of Robotics Research*, vol. 35, no. 4, pp. 422–434, Apr. 2016, doi: 10.1177/0278364915584806.

[19] H. Wang, B. Yang, Y. Liu, W. Chen, X. Liang, and R. Pfeifer, "Visual Servoing of Soft Robot Manipulator in Constrained Environments With an Adaptive Controller," *IEEE/ASME Trans. Mechatron.*, vol. 22, no. 1, pp. 41–50, Feb. 2017, doi: 10.1109/TMECH.2016.2613410.

[20] R. J. Webster and B. A. Jones, "Design and Kinematic Modeling of Constant Curvature Continuum Robots: A Review," *The International Journal of Robotics Research*, vol. 29, no. 13, pp. 1661–1683, Nov. 2010, doi: 10.1177/0278364910368147.

[21] M. Li, R. Kang, S. Geng, and E. Guglielmino, "Design and control of a tendon-driven continuum robot," *Transactions of the Institute of Measurement and Control*, vol. 40, no. 11, pp. 3263–3272, Jul. 2018, doi: 10.1177/0142331216685607.

[22] P. Qi, C. Liu, A. Ataka, H. K. Lam, and K. Althoefer, "Kinematic Control of Continuum Manipulators Using a Fuzzy-Model-Based Approach," *IEEE Trans. Ind. Electron.*, vol. 63, no. 8, pp. 5022–5035, Aug. 2016, doi: 10.1109/TIE.2016.2554078.

[23] W. S. Rone and P. Ben-Tzvi, "Mechanics Modeling of Multisegment Rod-Driven Continuum Robots," *Journal of Mechanisms and Robotics*, vol. 6, no. 4, p. 041006, Nov. 2014, doi: 10.1115/1.4027235.

[24] R. J. Webster, J. M. Romano, and N. J. Cowan, "Mechanics of Precurved-Tube Continuum Robots," *IEEE Trans. Robot.*, vol. 25, no. 1, pp. 67–78, Feb. 2009, doi: 10.1109/TRO.2008.2006868.

[25] D. C. Rucker and R. J. Webster III, "Statics and Dynamics of Continuum Robots With General Tendon Routing and External Loading," *IEEE Trans. Robot.*, vol. 27, no. 6, pp. 1033–1044, Dec. 2011, doi: 10.1109/TRO.2011.2160469.

[26] J. Till, V. Aloi, and C. Rucker, "Real-time dynamics of soft and continuum robots based on Cosserat rod models," *The International Journal of Robotics Research*, vol. 38, no. 6, pp. 723–746, May 2019, doi: 10.1177/0278364919842269.

[27] M. Giorelli, F. Renda, M. Calisti, A. Arienti, G. Ferri, and C. Laschi, "Neural Network and Jacobian Method for Solving the Inverse Statics of a Cable-Driven Soft Arm With Nonconstant Curvature," *IEEE Trans. Robot.*, vol. 31, no. 4, pp. 823–834, Aug. 2015, doi: 10.1109/TRO.2015.2428511.

[28] T. George Thuruthel, E. Falotico, M. Manti, A. Pratesi, M. Cianchetti, and C. Laschi, "Learning Closed Loop Kinematic Controllers for Continuum Manipulators in Unstructured Environments," *Soft Robotics*, vol. 4, no. 3, pp. 285–296, Sep. 2017, doi: 10.1089/soro.2016.0051.

[29] M. C. Yip and D. B. Camarillo, "Model-Less Feedback Control of Continuum Manipulators in Constrained Environments," *IEEE Trans. Robot.*, vol. 30, no. 4, pp. 880–889, Aug. 2014, doi: 10.1109/TRO.2014.2309194.

[30] M. Li, R. Kang, D. T. Branson, and J. S. Dai, "Model-Free Control for Continuum Robots Based on an Adaptive Kalman Filter," *IEEE/ASME Trans. Mechatron.*, vol. 23, no. 1, pp. 286–297, Feb. 2018, doi: 10.1109/TMECH.2017.2775663.

[31] Z. Hou and S. Jin, "Data-Driven Model-Free Adaptive Control for a Class of MIMO Nonlinear Discrete-Time Systems," *IEEE Trans. Neural Netw.*, vol. 22, no. 12, pp. 2173–2188, Dec. 2011, doi: 10.1109/TNN.2011.2176141.

[32] X. Li, C. Ren, S. Ma, and X. Zhu, "Compensated model-free adaptive tracking control scheme for autonomous underwater vehicles via extended state observer," *Ocean Engineering*, vol. 217, p. 107976, Dec. 2020, doi: 10.1016/j.oceaneng.2020.107976.

[33] K. Sun, M. Li, S. Wang, G. Zhang, H. Liu, and C. Shi, "Development of a Fiber Bragg Grating-Enabled Clamping Force Sensor Integrated on a Grasper for Laparoscopic Surgery," *IEEE Sensors J.*, vol. 21, no. 15, pp. 16681–16690, Aug. 2021, doi: 10.1109/JSEN.2021.3081444.

[34] Z. Tang, S. Wang, M. Li, and C. Shi, "Development of a Distal Tri-Axial Force Sensor for Minimally Invasive Surgical Palpation," *IEEE Trans. Med. Robot. Bionics*, vol. 4, no. 1, pp. 145–155, Feb. 2022, doi: 10.1109/TMRB.2022.3142361.